Inventory of Supplemental Information

SUPPLEMENTAL FIGURES

Figure S1. **Additional Characterization of *vam* Phenotypes, related to Figure 1**
A) Schematic showing the H (aa 4733-4900) and D (aa 4975-4993) regions of the Fat intracellular domain, locations of point mutations within the H region above, and deletions within the H region that impair Hippo activity below, including HM (4834-4899), PH (4733-4774), Hpo-N (4775-4836), Hpo-C (4839-4920), and H2 (4719-4900) (Bossuyt et al., 2014; Matakatsu and Blair, 2012; Pan et al., 2013; Zhao et al., 2013). We defined the ends of the H region (dashed lines) based on reports that deletions N-terminal to PH, or C-terminal to H2, did not impair Hippo rescuing activity in over-expression assays. (B,C) Adult male prothoracic legs from flies expressing *tub-Gal4 UAS-dcr2* (B) and *tub-Gal4 UAS-dcr2 UAS-vam-RNAi* (C). D) Quantification of relative tarsal lengths of the genotypes shown in B and C. Data are shown as mean ± SEM from measurements of 10-12 legs per genotype. **P* <0.001 (Student's *t* test). (E-H) Close up of proximal wing areas showing the orientation of hairs from wild-type control (E), vam^{c} (F), $vam^{c}/Df(2R)BSC345$ (G) and vam^{c}*; Vam-GFP* (H) flies. Arrows point to the regions where the hair orientation is disrupted. I-K) Hair polarity in the tergites of the wild-type control (I), vam^{c} (J) and d^{GC13}/d^{210} (K) mutant flies. Arrows point to regions where hair orientation is disrupted.

Figure S2. *vam* suppresses lethality, overgrowth and hair polarity phenotypes of *fat*, related to Figure 2
A-F,J) Close up of proximal wing areas showing hair polarity from flies carrying *nub-Gal4 UAS-Dcr2* (Control)(A), *nub-Gal4 UAS-Dcr2 UAS-Vam-RNAi* (B) *nub-Gal4 UAS-Dcr2 UAS-fat-RNA*i (C) *nub-Gal4 UAS-Dcr2 UAS-fat-RNAi UAS-Vam-RNAi* (D), *nub-Gal4 UAS-Dcr2 UAS-ds-RNA*i (E) *nub-Gal4 UAS-Dcr2 UAS-ds-RNAi UAS-Vam-RNAi* (F) $ft^{G\text{-}rv}$ vam^{c} homozygote (J). G-I) Hair polarity in tergites of wild-type control (G), trans-heterozygote $ft^{G\text{-}rv}/ft^{8}$ mutants (K) and homozygous $ft^{G\text{-}rv}$ vam^{c} mutant flies (I). K) Structure of Vam with the lowest C-score (-2.19) predicted by *ab initio* structure prediction program I-TASSER. L) Structural similarity of full length Vam with full length CRKII determined by TM-align structural alignment program of the I-TASSER suite. Ribbon diagram depicts the predicted structure of Vam and the magenta backbone trace depicts CRKII. TM alignment score is 0.831 and Coverage of alignment is 84.2%. M) Schematic depicting the predicted domain organization of Vam protein, with the numbers below denoting the amino acid numbers at the beginning and end of each SH3 domain.

Figure S3. Localization of Vam in the wing disc, related to Figure 3
A-C) Apical horizontal sections and vertical sections (as marked) of wing discs showing localization of *Vam:GFP* (green) relative to Dachs (red) (A,A',A''), Ds (red) (B,B, B'') and Fat (red) (C,C'C''), showing localization of Vam:GFP to the same apical plane as Dachs, Dachsous and Fat. D) Apical horizontal section from wing disc expressing D:GFP (green) and *nub-Gal4 UAS-Vam:RFP* (red). Overexpression of Vam leads to uniform distribution around the cell perimeter (D'').

Figure S4. Additional analysis of the relationship between Vam and Dachs, related to Figure 5
A,B) Horizontal apical sections of wing imaginal discs showing localization of D:GFP (green) and Fat (red) (A) or Ds (red) (B) in wing discs with vam^{c} mutant clones (marked by absence of RFP, blue). A slight cross-over from the RFP channel is visible in the panel examining Ds stain because of the high laser power required to visualize Ds in the wing. D:GFP puncta overlap Fat and Ds in wild-type cells, but not in vam^{c} mutant cells. C) Western blot showing total D:GFP levels, compared to GAPDH (control), in wing disc lysate from animals expressing *tub-Gal4,UAS-dcr2; D:GFP* or *tub-Gal4,UAS-dcr2; D:GFP UAS-Vam:RFP*. D-G) Adult male wings from flies expressing *nub-Gal4* alone (control) (D), *nub-Gal4 UAS-Dachs:V5* (E), *nub-Gal4 UAS-Vam:RFP* (F) and *nub-Gal4 UAS-Dachs:V5 UAS-vam-RFP* (G). (H) Quantification of the mean wing areas in flies of the genotypes shown in D-G, normalized to the control. Data shown as mean ± SEM from measurements of 10-12 wings per genotype. **P*<0.001(Student's *t* test between control and the different genotypes). I,J) Third instar wing imaginal discs expressing *en-Gal4 UAS-GFP*, *UAS-Vam:RFP* and *ex-lacZ* (I, I') or *ban-lacZ* (J, J') stained for expression of lacZ (magenta), with posterior cells marked by GFP (green). Dashed white line marks the A-P compartment boundary. K) Western blot showing levels of Vam-RFP relative to the loading control (Dcr2) in wing disc lysate from animals

expressing *nub-Gal4 UAS-Vam-RFP UAS-Dcr2* alone (control) or with *UAS-d-RNAi or UAS-fat-RNAi* with histograms showing quantitation from three different replicates. L) Western blot showing levels of D-GFP relative to the loading control (tubulin) in wing disc lysate from animals expressing *tub-Gal4; D-GFP UAS-Dcr2* (control) or with *UAS-vam-RNAi or UAS-fat-RNAi* with histograms showing quantitation from three different replicates. Error bars indicate sem.

Figure S5. Role of different domains and palmitoylation in Vam localization, related to Figure 6
A-C) Horizontal apical sections of wing discs expressing *nub-Gal4 and UAS-Vam-ΔSH3-1:RFP* (A,A'), *UAS-Vam-ΔSH3-3:RFP* (B,B'), or *UAS-Vam-N:RFP* (C,C'), showing their membrane localization. Full length Vam as well as Vam lacking any of the SH3 domains localizes to the apical region. For C) Vertical sections (below) show that the N-terminal region of Vam localizes to a both apical and baso-lateral membranes. D,E) Horizontal apical sections of wing imaginal discs expressing *Dachs:GFP* (D:GFP) *en-Gal4 UAS-CD8:RFP UAS-dcr2 UAS-Vam-RNAi* and *UAS-Vam-ΔSH3-1* (D,D') or *UAS-Vam-ΔSH3-3* (E,E'), showing rescue of D:GFP (green) membrane localization in the posterior compartments by Vam-ΔSH3-1:RFP or Vam-ΔSH3-3:RFP. Dashed white line marks edge of en-Gal4 expression. F) Horizontal apical sections of wing discs expressing, *en-Gal4 UAS-dcr2, UAS-app-RNAi; Vam:GFP* showing the loss of membrane localization of Vam:GFP in the posterior compartment. G) Western blot showing acyl biotin exchange (ABE) assay for V5-tagged wild-type or mutant (C5S) Vam. Vam does not get biotinylated in the ABE assay. A protein that shows biotinylation (red) is higher in molecular weight than Vam and is not stained with anti V5 antibody (green). H,I) Horizontal and vertical (at left) sections of wing imaginal discs expressing *nub-Gal4 UAS-Vam:GFP* (H, H') or *UAS-Vam-(CS):GFP* (I, I') showing their relative localization, stained for E-cad (red) and DNA (Hoechst, magenta). Compared to Vam:GFP, Vam-CS:GFP is detected at higher levels in the cytoplasm.

Figure S6. **Influence of the H region of the Fat intracellular domain on Vam and Dachs localization, related to Figure 7**
Horizontal apical sections of wing imaginal discs expressing either *en-Gal4; D:GFP (A-D) or hh-Gal4 act>vam:GFP* (E-G) or *en-Gal4 vam:GFP* (H) *and UAS-Fat- ΔECD* (A,A',E,E'), *UAS-Fat-ΔECD-Δ5-C* (B, B',F,F'), *UAS-Fat-ΔECD-Δ3-5* (C,C',G,G') and *UAS-Fat^{3Only} (*D,D',H,H') showing their influence on apical membrane localization of D:GFP and Vam:GFP in posterior cells (at right, marked in panels without prime symbols by red stain). I) Western blot showing results of co-immunoprecipitation by RFP-trap of V5-tagged GFP (negative control), V5-tagged Fat-ICD, V5-tagged Fat-ΔH2 or V5-tagged Fat-H2 (detected by anti-V5), co-expressed in S2 cells with Vam:RFP. J) Western blot showing results of co-immunoprecipitation by RFP-trap of V5-tagged GFP (negative control), V5-tagged Fat-ICD or V5-tagged Fat-ICD-C (detected by anti-V5), co-expressed in S2 cells with Vam:RFP. K) Schematic showing constructs analyzed in panels I,J.

Figure S7. **Localization of the different Fat constructs, related to Figure 7**
Horizontal apical sections of wing imaginal discs expressing either *en-Gal4; D:GFP or hh-Gal4 act>vam:GFP* (A-N) or *en-Gal4 vam:GFP* (P) *and UAS-Fat-FL* (A,B), *UAS-Fat-ΔH2* (C,D), *UAS-Fat-ΔECD* (E, F), *UAS-Fat-ΔECD-Δ6-C* (G,H), *UAS-Fat-ΔECD-Δ5-6* (I,J), *UAS-Fat-ΔECD-Δ5-C* (K,L), *UAS-Fat-ΔECD-Δ3-5* (M,N) and *UAS-Fat^{3Only}* (O,P) showing their localization in posterior cells (at right, marked by red stain).

Misra & Irvine Figure S1

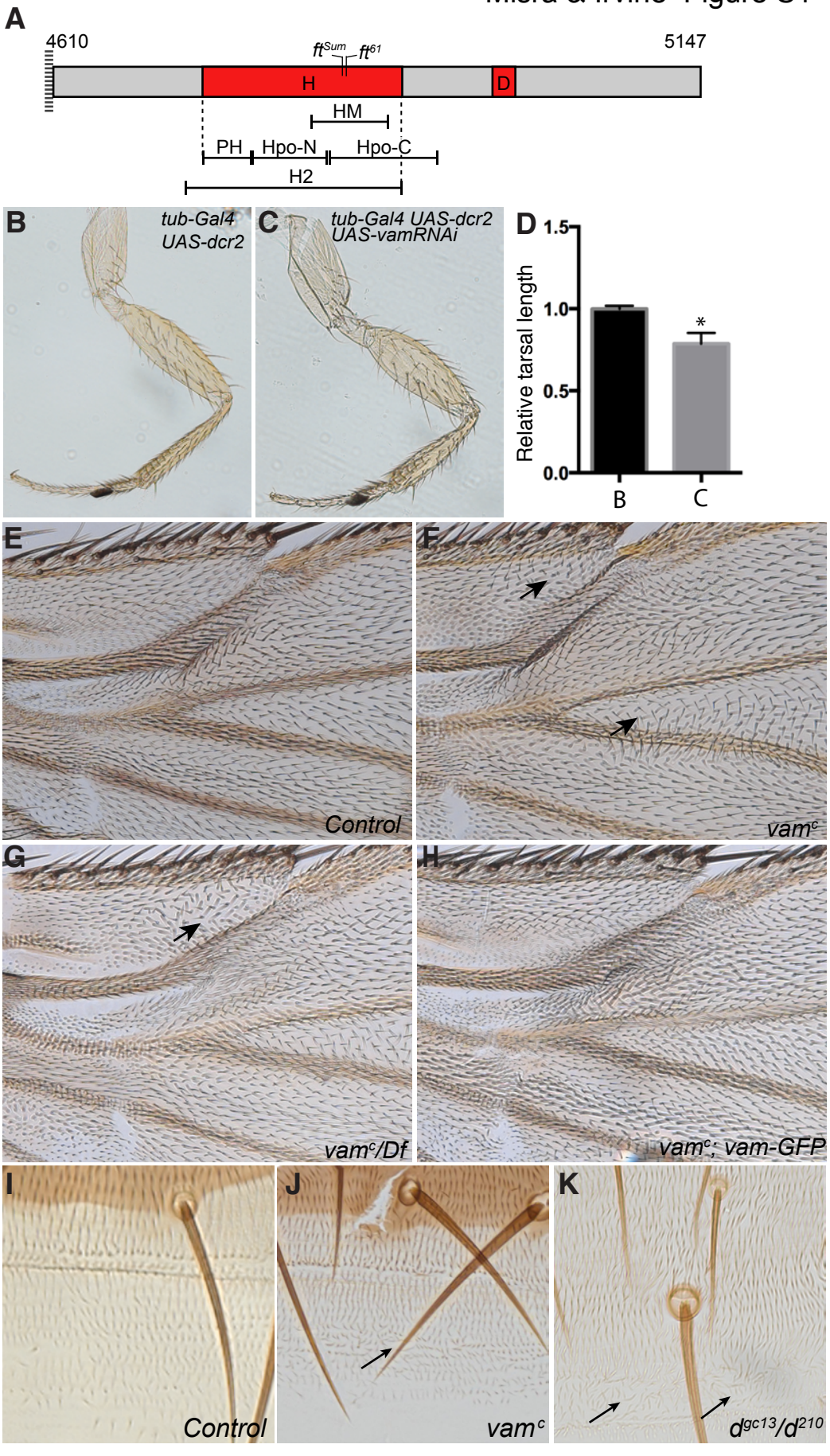

Misra & Irvine Figure S2

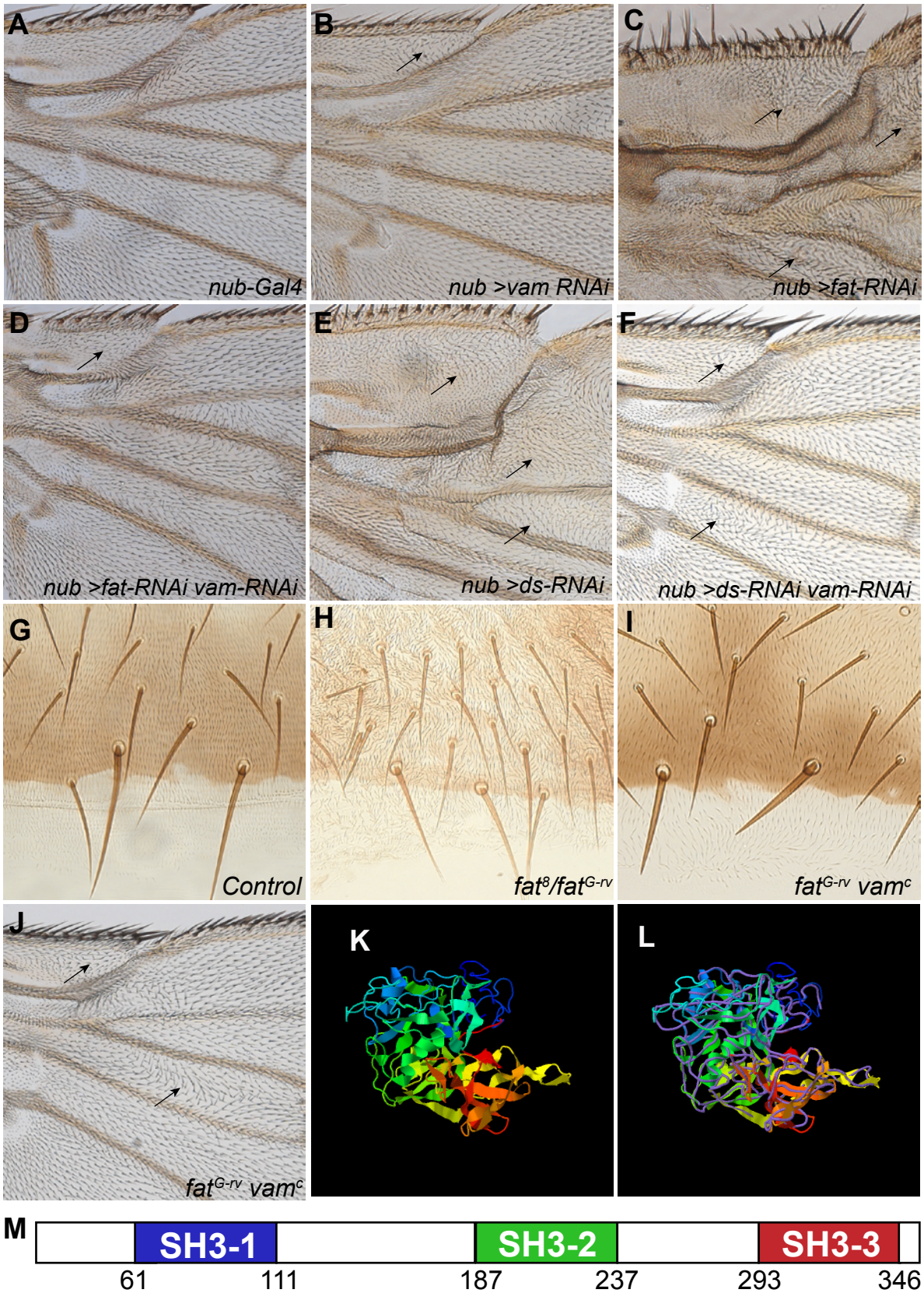

Misra & Irvine Fig. S3

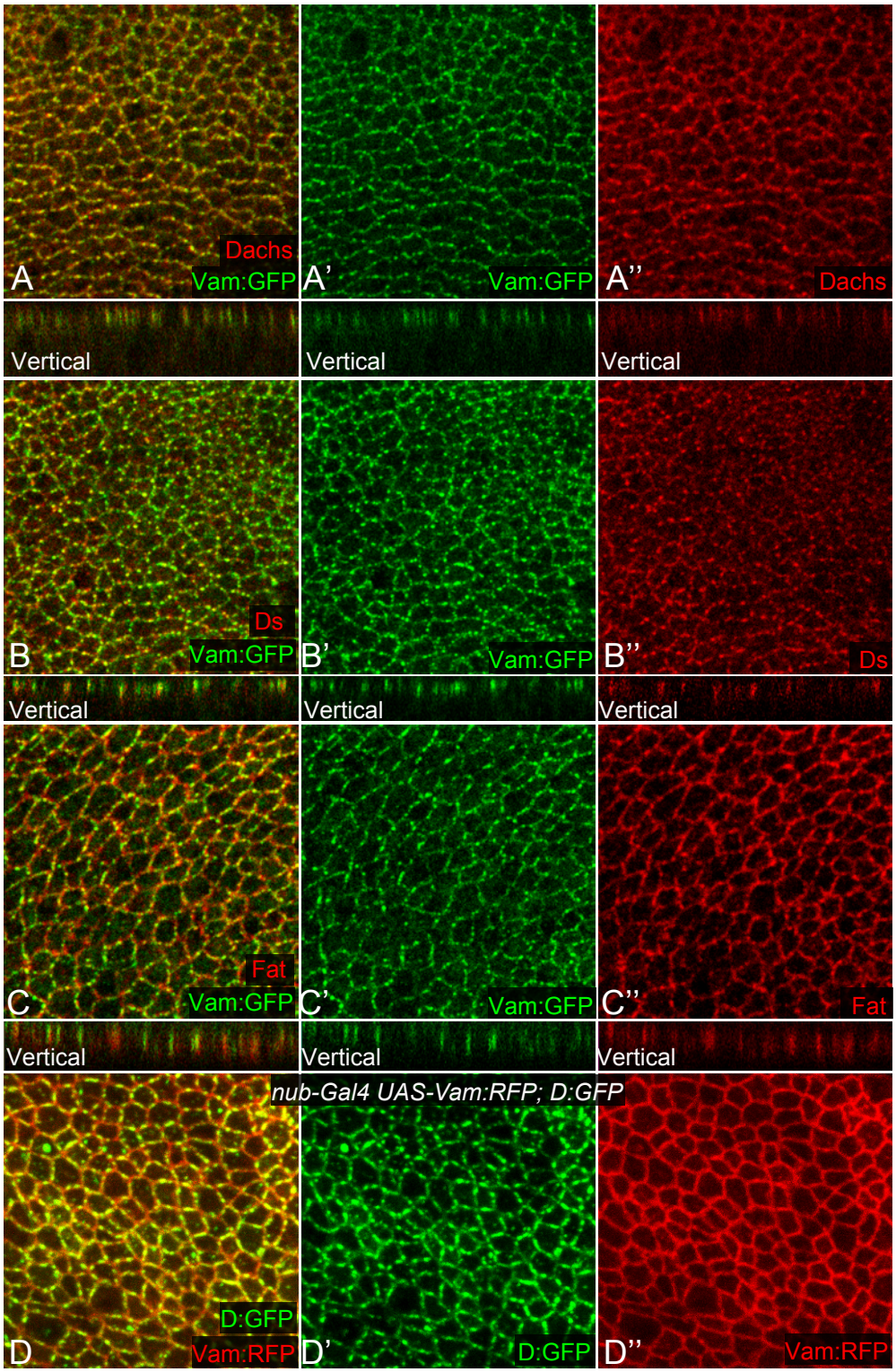

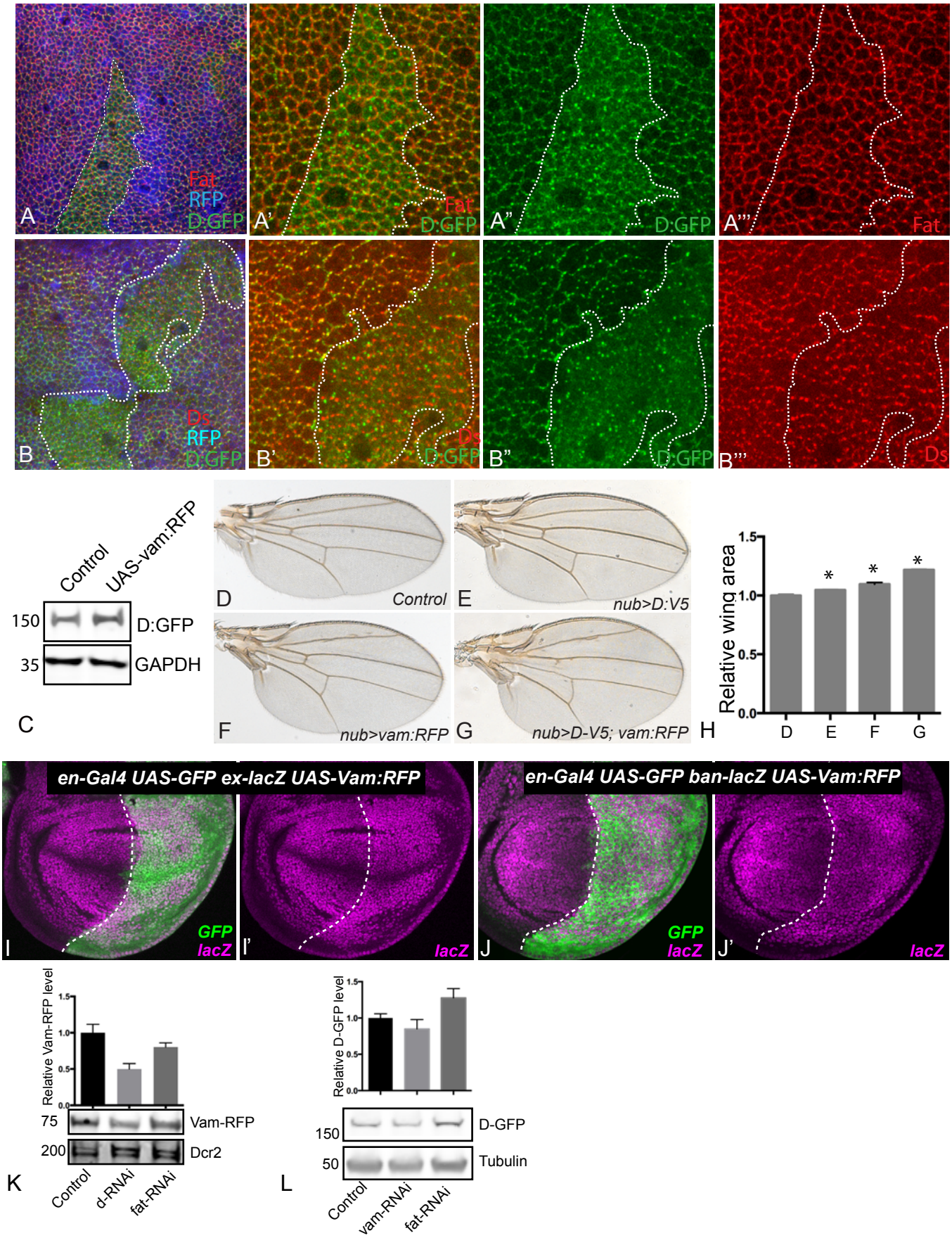
A
Fat
RFP
D:GFP
A'
Fat
D:GFP
A"
D:GFP
A"'
Fat
B
Ds
RFP
D:GFP
B'
Ds
D:GFP
B"
D:GFP
B"'
Ds
Control
UAS-vam:RFP
150
D:GFP
35
GAPDH
C
D
Control
E
nub>D:V5
F
nub>vam:RFP
G
nub>D-V5; vam:RFP
H
Relative wing area
1.5
1.0
0.5
0.0
*
*
*
D
E
F
G
en-Gal4 UAS-GFP ex-lacZ UAS-Vam:RFP
GFP
lacZ
I
I'
lacZ
en-Gal4 UAS-GFP ban-lacZ UAS-Vam:RFP
GFP
lacZ
J
J'
lacZ
Relative Vam-RFP level
1.5
1.0
0.5
0.0
75
Vam-RFP
200
Dcr2
Control
d-RNAi
fat-RNAi
K
Relative D-GFP level
1.5
1.0
0.5
0.0
150
D-GFP
50
Tubulin
Control
vam-RNAi
fat-RNAi
L

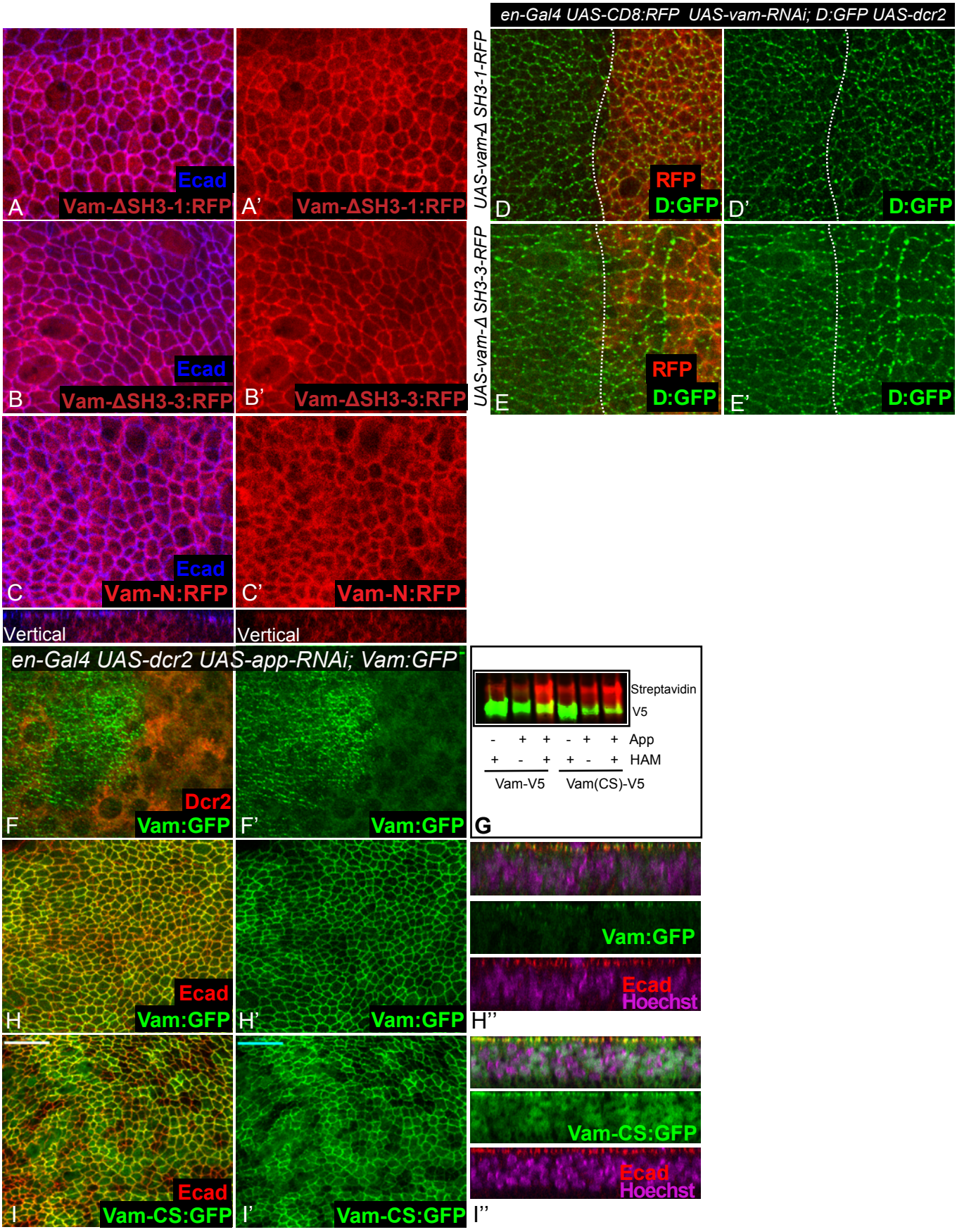
en-Gal4 UAS-CD8:RFP UAS-vam-RNAi; D:GFP UAS-dcr2
UAS-vam-Δ SH3-1-RFP
UAS-vam-Δ SH3-3-RFP
A
Ecad
Vam-ΔSH3-1:RFP
A'
Vam-ΔSH3-1:RFP
B
Ecad
Vam-ΔSH3-3:RFP
B'
Vam-ΔSH3-3:RFP
C
Ecad
Vam-N:RFP
C'
Vam-N:RFP
Vertical
Vertical
D
RFP
D:GFP
D'
D:GFP
E
RFP
D:GFP
E'
D:GFP
en-Gal4 UAS-dcr2 UAS-app-RNAi; Vam:GFP
F
Dcr2
Vam:GFP
F'
Vam:GFP
Streptavidin
V5
- + + - + + App
+ - + + - + HAM
Vam-V5
Vam(CS)-V5
G
H
Ecad
Vam:GFP
H'
Vam:GFP
Vam:GFP
Ecad
Hoechst
H''
I
Ecad
Vam-CS:GFP
I'
Vam-CS:GFP
Vam-CS:GFP
Ecad
Hoechst
I''

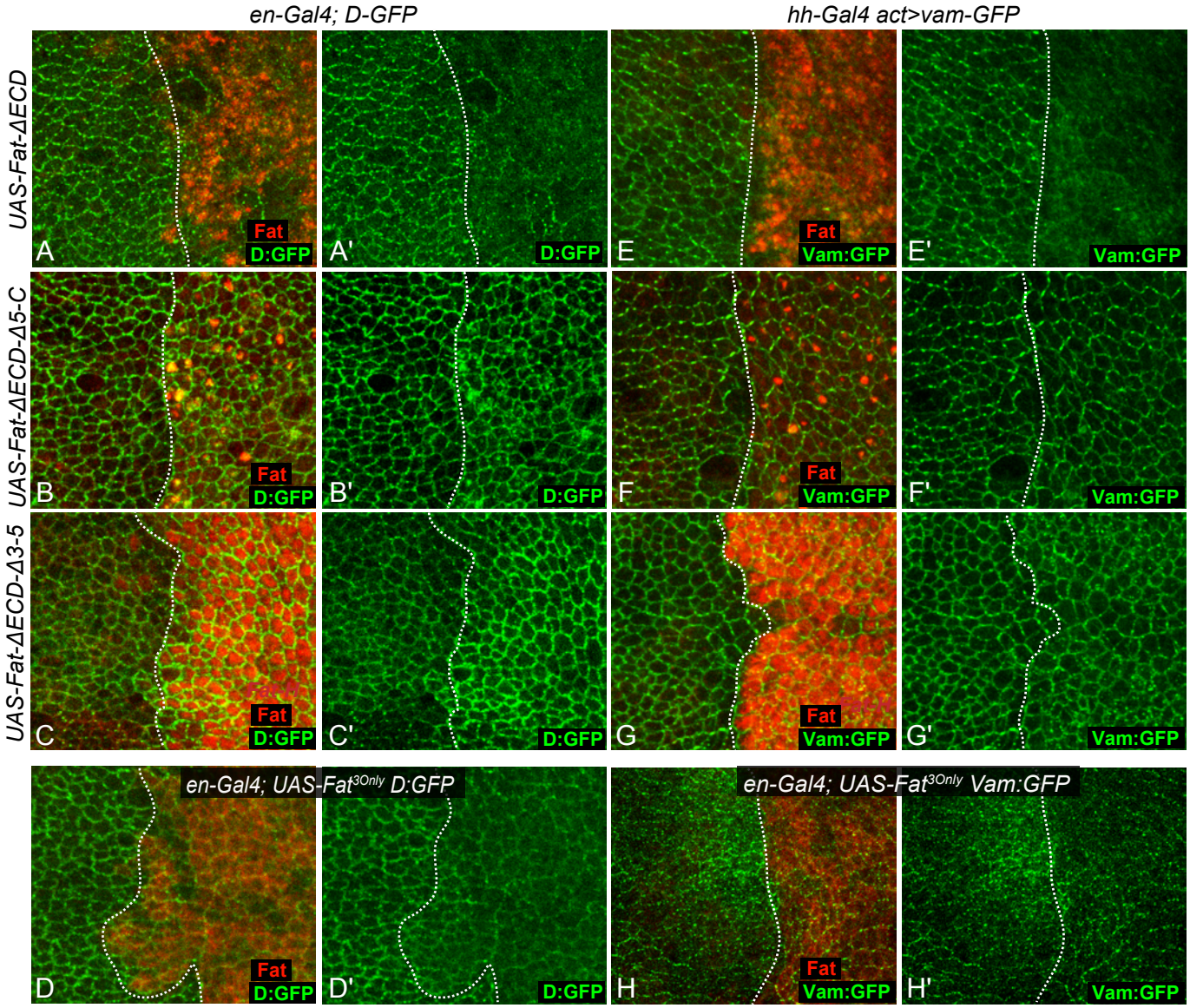
en-Gal4; D-GFP
hh-Gal4 act>vam-GFP
UAS-Fat-ΔECD
UAS-Fat-ΔECD-Δ5-C
UAS-Fat-ΔECD-Δ3-5
A
A'
B
B'
C
C'
D
D'
E
E'
F
F'
G
G'
H
H'
Fat
D:GFP
Vam:GFP
en-Gal4; UAS-Fat3Only D:GFP
en-Gal4; UAS-Fat3Only Vam:GFP

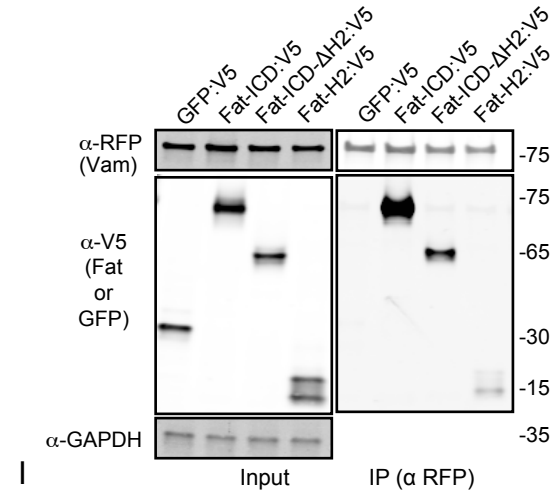
GFP:V5
Fat-ICD:V5
Fat-ICD-ΔH2:V5
Fat-H2:V5
α-RFP (Vam)
α-V5 (Fat or GFP)
α-GAPDH
-75
-65
-30
-15
-35
Input
IP (α RFP)
I

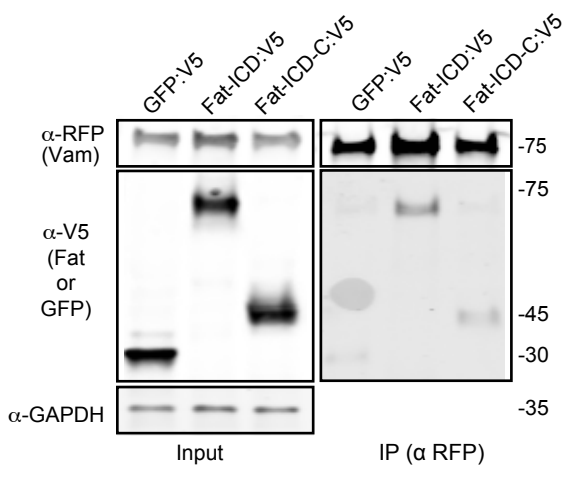
GFP:V5
Fat-ICD:V5
Fat-ICD-C:V5
α-RFP (Vam)
α-V5 (Fat or GFP)
α-GAPDH
-75
-45
-30
-35
Input
IP (α RFP)
J

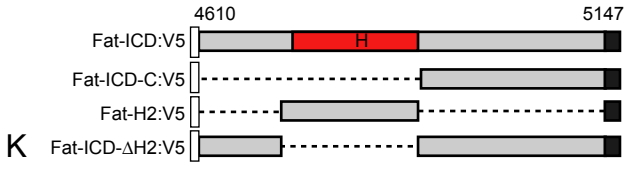
4610
5147
H
Fat-ICD:V5
Fat-ICD-C:V5
Fat-H2:V5
Fat-ICD-ΔH2:V5
K

Misra & Irvine Figure S7

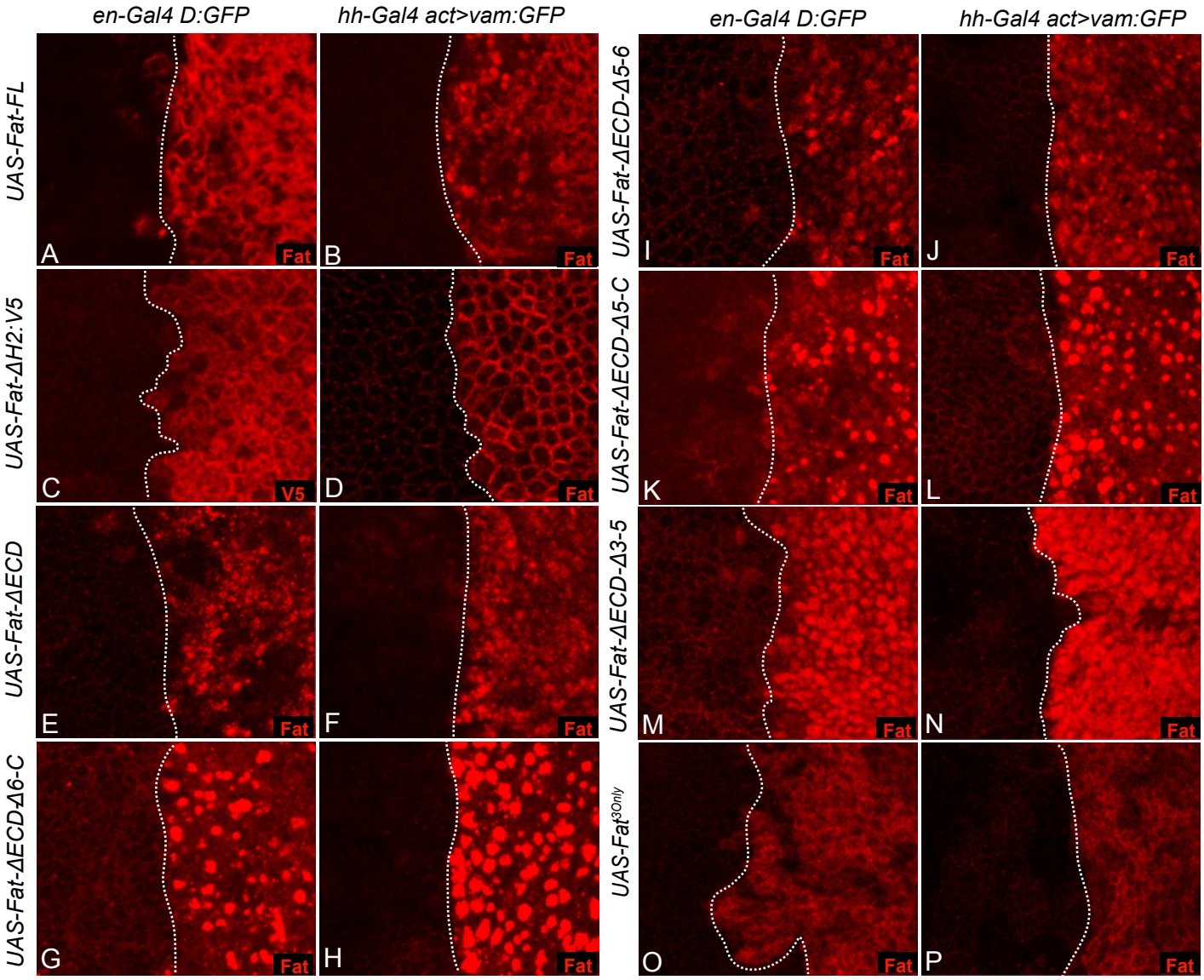

SUPPLEMENTAL EXPERIMENTAL PROCEDURES

Generation of *vam*^{c}

The *vam*^{c} mutant was generated by replacement of the *vam* coding region by 3xP3-DsRed by recombination mediated cassette exchange assisted by CRISPR-Cas9 (Bassett and Liu, 2014). Briefly, gRNAs were designed using the CRISPR Optimal Target Finder tool (Gratz et al., 2014) and oligos encoding gRNA1 (forward 5' CTTCGAAGGGGGTTTAATTCCGAG3' and reverse 5'AAACCTCGGAATTAAACCCCCTTC3') and gRNA2 (forward 5'CTTCGAAATGCAATTCGACTGTGTT3'and reverse 5' AAACAACACAGTCGAATTGCATTTC3') were annealed and ligated to pU6 plasmid digested with BbsI. Left homology arm was amplified by PCR using the primers forward 5' TTCGCTGAA GCAGGTGGAATTCTCATAGCGCCTGGAGCTAACTC 3' and reverse 5' GCCGCTAGCATGCAAGAATTCTCGGCTAATTGCTTAATTTCTTTATTGTTTAGATCC 3'. Similarly, the right homology arm was amplified by PCR using the primers, forward 5' CTAGGCCTTCTGCAGCTCGAGCGAAAAGCGTTTCTTTGTGGCTTGG3' and reverse 5' GATTGACGGAAGAGCCTCGAGGAGAATCCGGAGACCAACGACTATT 3'. The left and right homology arms were simultaneously cloned into the EcoRI and XhoI sites in the MCS1 and MCS2 respectively of the plasmid pHD-DsRed-attp. The plasmids pU6-gRNA1 and pU6-gRNA2 along with pHD-DsRed-attp containing the left and right homology arms, were injected into embryos from flies expressing CAS-9 under the control of *nos* promoter and progeny expressing the DS-Red in the eye were selected. The replacement of the *vam* locus by the 3xP3-DsRed cassette was verified by PCR and DNA sequencing.

Viability of Mutant Flies

Viability of semi-lethal genotypes is calculated by comparing numbers of flies eclosing to numbers expected for a wild-type chromosome, which for a cross between mutations over a recessive lethal balancer chromosome is one third of the total.

Molecular Biology

vam cDNA was PCR amplified with forward primer 5'TGAATAGGGAATTGGGAATTC ATGGCATTTCTTTGCCCCGTG3' vam-3xFLAG rev 5'CCGTCATGGTCTTTGTAGTCAAGGCTGGTCATCGCGGG3'. 3x-FLAG-GFP was amplified with Forward primer 5'GACTACAAAGACCATGACGGTGATTATAAAGATCATGACATCG ATTACAAGGATGACGATGACAAGATGGTGAGCAAGGGCGAGG3' and reverse primer 5' GCGGCCGCAAGATCTGTTAACGAATTCTTACTTGTACAGCTCGTCCATGCC3'. These fragments were cloned into attb-pUAST plasmid digested with EcoRI, by Gibson assembly to create pUAST-Vam-3X-FLAG-EGFP. pUAST-Vam-3X-FLAG-tRFP was created in a similar manner, where 3xFLAG-tRFP was amplified with 5'GACTACAAAGACCATGACGGTGATTATA AAGATCATGACATCGATTACAAGGATGACGATGACAAGATGGTGTCTAAGGGCGAAGAGC3' and reverse primer 5'GCGGCCGCAAGATCTGTTAACGAATTCTTAATTAAGTTTGTGCCCC AGTTTGCT3'. To create Vam-C5S, the mutation was introduced in the forward primer. For making the delta SH3 constructs, G-block fragments that encode either the individual SH3 domains or Vam-3x-FLAG without amino acids 61-111 (SH3-1) 187-237 (SH3-2) or 293-346 (SH3-3) were synthesized by IDT and cloned in frame with 3X-FLAG-TRFP by Gibson assembly into attb-PUAST. pUAST-Vam-ΔSH3-1-3x-FLAG-RFP and Vam-ΔSH3-2-3x-FLAG-RFP constructs were rendered RNAi resistant by introducing synonymous mutations into the coding region targeted by the RNAi line (CTGTATGATTACAAAGCGCAA-to CTCTACGACTACAAGGCTCAG). In pUAST-Vam-ΔSH3-3-3x-FLAG-RFP this sequence is deleted. Vam genomic GFP was constructed as described previously (Venken et al., 2008). Briefly, the FRT-Kan-FRT-EGFP sequence was amplified from pL452-cEGFP with forward primer 5'CCCGCAAATATGGATTCATCCCGAAAGCCTATGCCCGACCACCCGCGATGACCAGCCTT GCAGCCCAATTCCGATCATATTC3' and reverse primer 5'CGCTTTAGTGTTAGTCGAAGTGA TAATTAAAACGATTATGGTATTGAATCTATTTCTTA TTACTTGTACAGCTCGTCCATG3' that contain homology sequences for recombination. Recombination of attb-pacman-BAC-CH322-181F05 was performed using *E.coli* strain SW106. To create attb-pACT-FRT-Stop-FRT-vam-3x-FLAG-GFP, Vam-3X-FLAG-GFP was amplified with forward primer 5'GAGATCCCCCGGGCTGCAGGAATTC ATGGCATTTCTTTGCCCCGTG3' and reverse primer 5'CTGACGGTGCAAAATGCTCGCATGAATTCTTACTTGTACAGCTCGTCCATGCC3' and cloned by Gibson assembly, into attb-pAct-FRT-Stop-FRT (Brittle et al., 2010) digested with EcoRI,. To create pUAST-Fat-H2- a fragment encoding the transmembrane domain was PCR amplified with Fat-for 5'TAGTCCAGTGTGGTGGAATTCATGGAGAGGCTACTGCTCCTGT3' and Fat-H2-rev1-5'GCGGAATGGGCAGGTGATGACTCAAACTACCAATCTTCTCCTGCT3', and

a fragment encoding the H2 region was PCR amplified with Fat-H2-for-
5'GAGAAGATTGGTAGTTTGAGTCATCACCTGCCCATTCCGC3'
Fat H2-rev- 5'GCAAGATCTGTTAACGAATTCTCAATGGTGATGGTGATGATGACCG3' and cloned into EcoRI site in the pUAST plasmid by Gibson assembly. To create pUAST-Fat-ICD-C-V5 a fragment encoding the Fat transmembrane domain was PCR amplified with Fat-for 5'TAGTCCAGTGTGGTGGAATTCATGGAG AGGCTACTGCTCCTGT3' and Fat-C-rev-5' ACTCAAACTACCAATCTTCTCCTGCT 3', and a fragment encoding the C terminal region of Fat was PCR amplified with Fat-C-for- 5' ATTGGTAGTTTGAGTAGTTCCAGTGCCAGCAGGC 3' and Fat-rev 5'GCAAGATCTGT TAACGAATTCTCAATGGTGATGGTGATGATGACCG 3' and cloned into the EcoRI site in the pUAST plasmid by Gibson assembly.

SUPPLEMENTAL REFERENCES

Bassett, A.R., and Liu, J.-L. (2014). CRISPR/Cas9 and genome editing in Drosophila. J Genet Genomics *41*, 7–19.

Brigidi, G.S., and Bamji, S.X. (2013). Detection of protein palmitoylation in cultured hippocampal neurons by immunoprecipitation and acyl-biotin exchange (ABE). J Vis Exp.

Brittle, A.L., Repiso, A., Casal, J., Lawrence, P.A., and Strutt, D. (2010). Four-jointed modulates growth and planar polarity by reducing the affinity of dachsous for fat. Curr. Biol. *20*, 803–810.

Feng, Y., and Irvine, K.D. (2009). Processing and phosphorylation of the Fat receptor. Proceedings of the National Academy of Sciences *106*, 11989–11994.

Gratz, S.J., Ukken, F.P., Rubinstein, C.D., Thiede, G., Donohue, L.K., Cummings, A.M., and O'Connor-Giles, K.M. (2014). Highly specific and efficient CRISPR/Cas9-catalyzed homology-directed repair in Drosophila. Genetics *196*, 961–971.

Kumari, B., Kumar, R., and Kumar, M. (2014). PalmPred: an SVM based palmitoylation prediction method using sequence profile information. PloS One *9*, e89246.

Mao, Y., Kucuk, B., and Irvine, K.D. (2009). Drosophila lowfat, a novel modulator of Fat signaling. Development *136*, 3223–3233.

Mao, Y., Rauskolb, C., Cho, E., Hu, W.L., Hayter, H., Minihan, G., Katz, F.N., and Irvine, K.D. (2006). Dachs: an unconventional myosin that functions downstream of Fat to regulate growth, affinity and gene expression in Drosophila. Development *133*, 2539–2551.

Merkel, M., Sagner, A., Gruber, F.S., Etournay, R., Blasse, C., Myers, E., Eaton, S., and Jülicher, F. (2014). The Balance of Prickle/Spiny-Legs Isoforms Controls the Amount of Coupling between Core and Fat PCP Systems. Curr. Biol. *24*, 2111–2123.

Rauskolb, C., Pan, G., Reddy, B.V., Oh, H., and Irvine, K.D. (2011). Zyxin links fat signaling to the hippo pathway. PLoS Biol *9*, e1000624.

Rauskolb, C., Sun, S., Sun, G., Pan, Y., and Irvine, K.D. (2014). Cytoskeletal tension inhibits Hippo signaling through an Ajuba-Warts complex. Cell *158*, 143–156.

Ren, J., Wen, L., Gao, X., Jin, C., Xue, Y., and Yao, X. (2008). CSS-Palm 2.0: an updated software for palmitoylation sites prediction. Protein Eng. Des. Sel. *21*, 639–644.

Schwank, G., Tauriello, G., Yagi, R., Kranz, E., Koumoutsakos, P., and Basler, K. (2011). Antagonistic growth regulation by Dpp and Fat drives uniform cell proliferation. Dev Cell *20*, 123–130.

Venken, K.J.T., Kasprowicz, J., Kuenen, S., Yan, J., Hassan, B.A., and Verstreken, P. (2008). Recombineering-mediated tagging of Drosophila genomic constructs for in vivo localization and acute protein inactivation. Nucleic Acids Research *36*, e114.

Yang, J., Yan, R., Roy, A., Xu, D., Poisson, J., and Zhang, Y. (2015). The I-TASSER Suite: protein structure and function prediction. Nat. Methods *12*, 7–8.